Gas Mixing and Modeling of Secondary Gas Distribution in a Bench-Scale Fluidized Bed

Fahad Al-Sherehy, John Grace, and Alaa-Eldin Adris
Dept. of Chemical and Biochemical Engineering, University of British Columbia, Vancouver, Canada V6T 1Z4

DOI 10.1002/aic.10090
Published online in Wiley InterScience (www.interscience.wiley.com).

The effect of distributing gaseous feed along a bubbling fluidized bed of diameter 152 mm was studied with fluid catalytic cracking particles. Steady- and unsteady-state experiments show that the secondary gas concentration profile at the injection level was almost uniform for high secondary and low primary gas velocities. Secondary gas readily mixed within a short distance above the injection level. Backmixing was primarily influenced by the primary feed superficial gas velocity. Regardless of its injection velocity, secondary gas was barely detectable below the injection level at low primary superficial velocities. Axial dispersion and mass transfer decreased significantly when some gas was introduced at higher levels, compared with a bed where all gas entered through the windbox. Two two-phase models are proposed to simulate gas mixing, the first with a step-change in gas flow rate at the injection level, the second accounting for additional mixing in the jet region. © 2004 American Institute of Chemical Engineers *AIChE J,* 50: 922–936, 2004
Keywords: fluidization, jets, gas mixing, modeling, secondary feed

Introduction

Several industrial fluid bed processes introduce gaseous reactants along the reactor height rather than only through the distributor at the bottom (Bramer, 1995; Contractor and Sleight, 1988; Yates et al., 1987). Distributed feed may improve the selectivity of a process involving consecutive reactions. Another important motivation is to maintain the composition of the reactor feed mixture outside explosion limits. Different configurations can be used to introduce a reactant into a reactor in a controlled manner. Examples include membranes (Coronas et al., 1995; Tonkovich et al., 1996) and direct injection as jets through injection points (Choudhary et al., 1989) at different levels, in addition to gas entering through the bottom distributor.

Mixing is an important aspect in fluidized bed processes. When chemical reactions occur, concentration profiles differ in the bubble phase and dense phase. The extent of reaction depends on the rate of exchange of gas between the phases (e.g., between the bubble and dense phases for bubbling fluidized beds). The net rate of exchange of gas depends on the concentration difference, which is affected by the state of mixing (Potter, 1971). In addition, the overall conversion and selectivity within each phase are influenced by the degree of axial dispersion in that phase.

The present study is focused on gas mixing in fluidized beds operating in the bubbling regime. The mixing is considered for two design configurations. In the first, all gas is fed through the windbox. In the second, part of the gaseous feed (designated primary gas) is introduced through the windbox, whereas the rest (denoted as secondary gas) is distributed along the bed height. The objective of this work is to evaluate the impact of distributing the secondary gas along the bed height on the gas mixing. Gas mixing in fluidized beds without secondary gas has been well studied since the 1950s, although configurations with distributed gas injection have not been widely investigated. In the present article, all secondary gas is injected through a single nozzle in a relatively small column. Cases with multiple secondary jets will be considered in future articles.

Correspondence concerning this article should be addressed to J. Grace at jgrace@chml.ubc.ca.

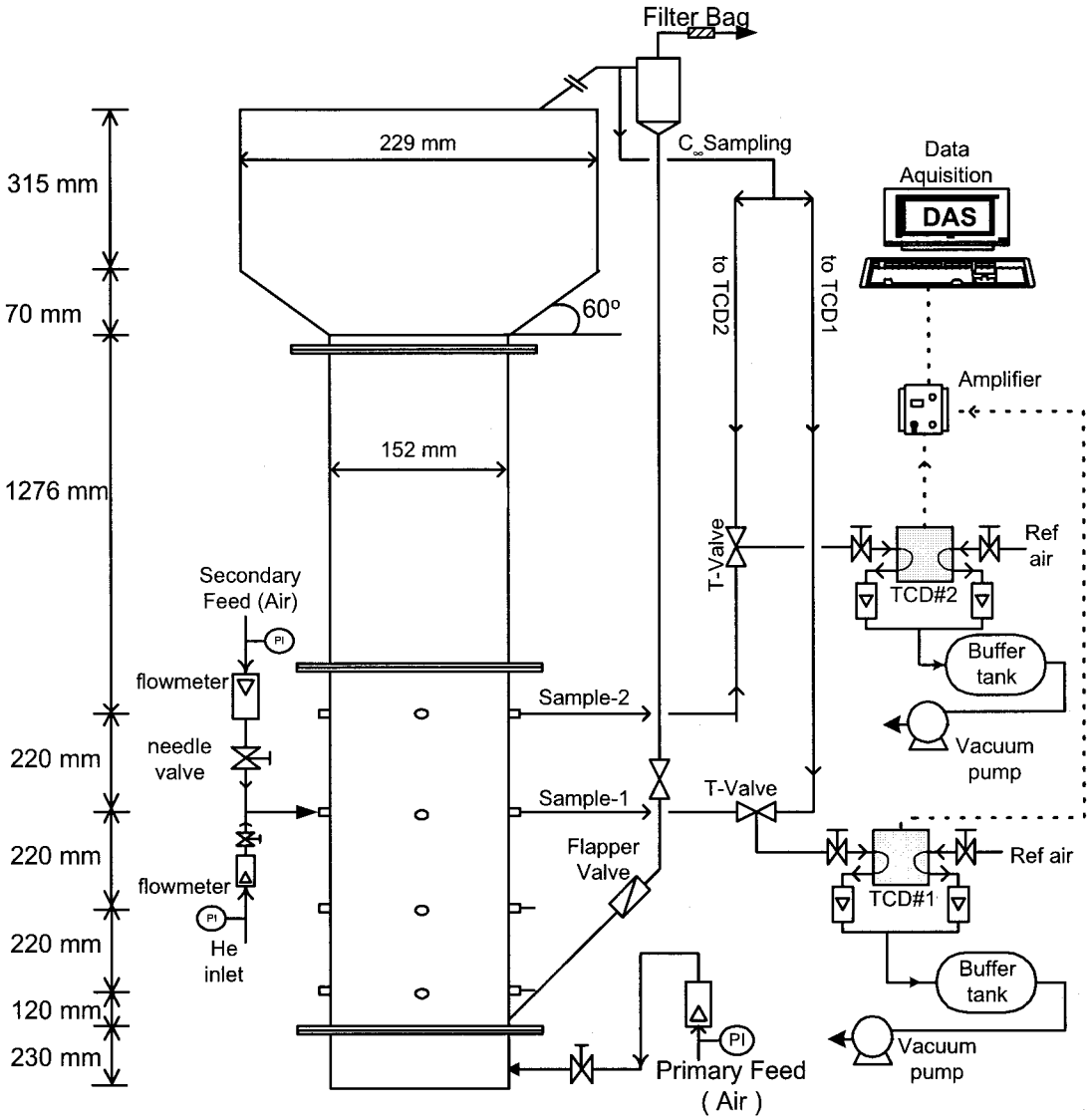

Figure 1. Steady-state tracer injection/detection set-up (not to scale).

When gas is introduced along the height of a fluid bed reactor, its distribution is likely to affect the reactor performance: (1) by progressively changing the composition of the reacting mixture, and (2) by changing the flow pattern and hydrodynamics in the bed, both attributed to the secondary jets and to the variation of total flow with height. Aside from interest in secondary air associated with addition of secondary air in circulating fluidized bed combustion to reduce NO_x emissions (e.g., see Grace, 1997) and the study of Lummi and Baskakov (1967), who injected a CO_2 tracer with a horizontal air jet and measured subsequent CO_2 concentrations in the bed, no previous work appears to have been reported on how distributed feed affects gas mixing.

When a gas jet is injected horizontally into a fluidized bed, there are four possible modes of discharge into the bed: bubbling at the near wall where the gas is injected, bubbling inside the bed, jetting terminating within the bed, and jet penetration right across to the opposite wall facing the injection nozzle. Which mode occurs in a given case depends on the secondary gas injection velocity, primary gas flow, particle properties, and column width or diameter. The mode of injection influences many aspects of behavior inside the bed, for example, gas-solid contacting, gas and solid mixing, residence time distribution (RTD), and uniformity of secondary gas concentration.

Experimental Apparatus and Instrumentation

Gas mixing experiments were carried out in the equipment shown schematically in Figure 1, featuring a cylindrical column, made in two sections, a main (lower) section of 152-mm inside diameter (ID) and 2286 mm height and an expanded (upper) section of 229 mm ID and 315 mm height, connected by a smooth conical transition. The column was constructed of transparent cast acrylic (PlexiGlas). Rotameters provided flow measurements for the main feed and for each injection level. A data-acquisition system (DASH-8 A-D converter, EXP-16

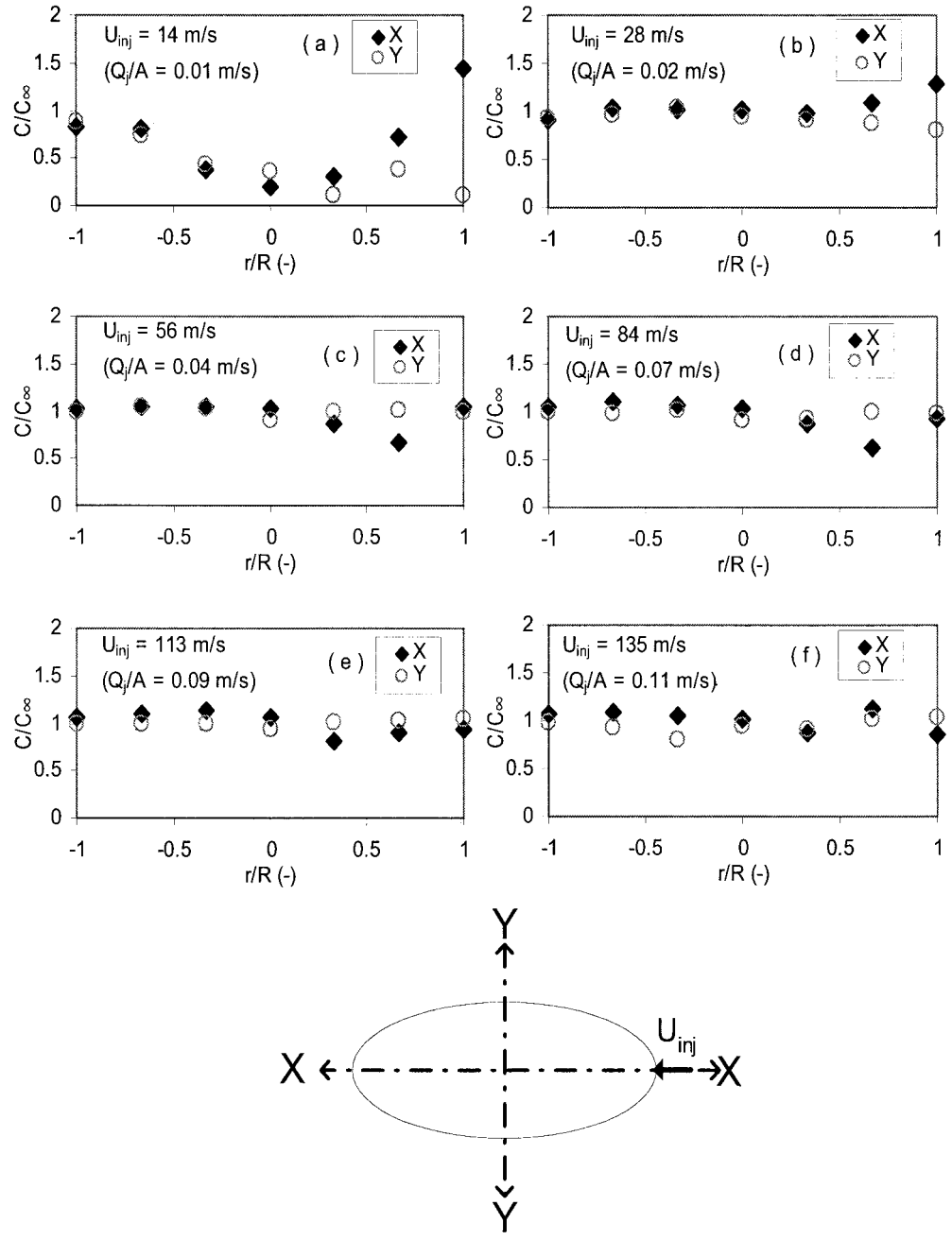

Figure 2. Radial tracer concentration profiles along parallel and perpendicular diameters at the same level as secondary injection for different secondary air injection velocities (U_{inj}). U_P = 0.01 m/s; H_0 = 1,100 mm; tracer injection at z_j = 560 mm.

multiplexer and Pentium-II personal computer) monitored pressure transducer and gas concentration signals.

The key properties of the fluid catalytic cracking (FCC) particles used in the experiments were: ρ_p = 1460 kg/m^3 (catalyst supplier); $\overline{d_p}$ = 61 μm (Sauter mean, sieve analysis); ε_{mf} = 0.48 (measured); U_{mf} = 3.0 mm/s (measured). Air was the fluidizing gas, and the bed was operated at ambient temperature and pressure. Helium was used as tracer, with transient step injection for RTD measurements, or with continuous injection for backmixing and distribution profile experiments. Helium was ideal because it is inert, nonadsorbing and readily detectable. A nonadsorbing tracer allows study of that portion of the mixing that is solely related to the hydrodynamics. The tracer concentrations at prechosen positions were monitored by sampling with the aid of thermal conductivity detectors (TCD) assembled in our laboratory (Al-Sherehy, 2002).

Steady-State Measurements

The distribution of the secondary gas inside the bed was examined by adding a steady flow of helium tracer to the secondary air injected 560 mm above the distributor, dis-

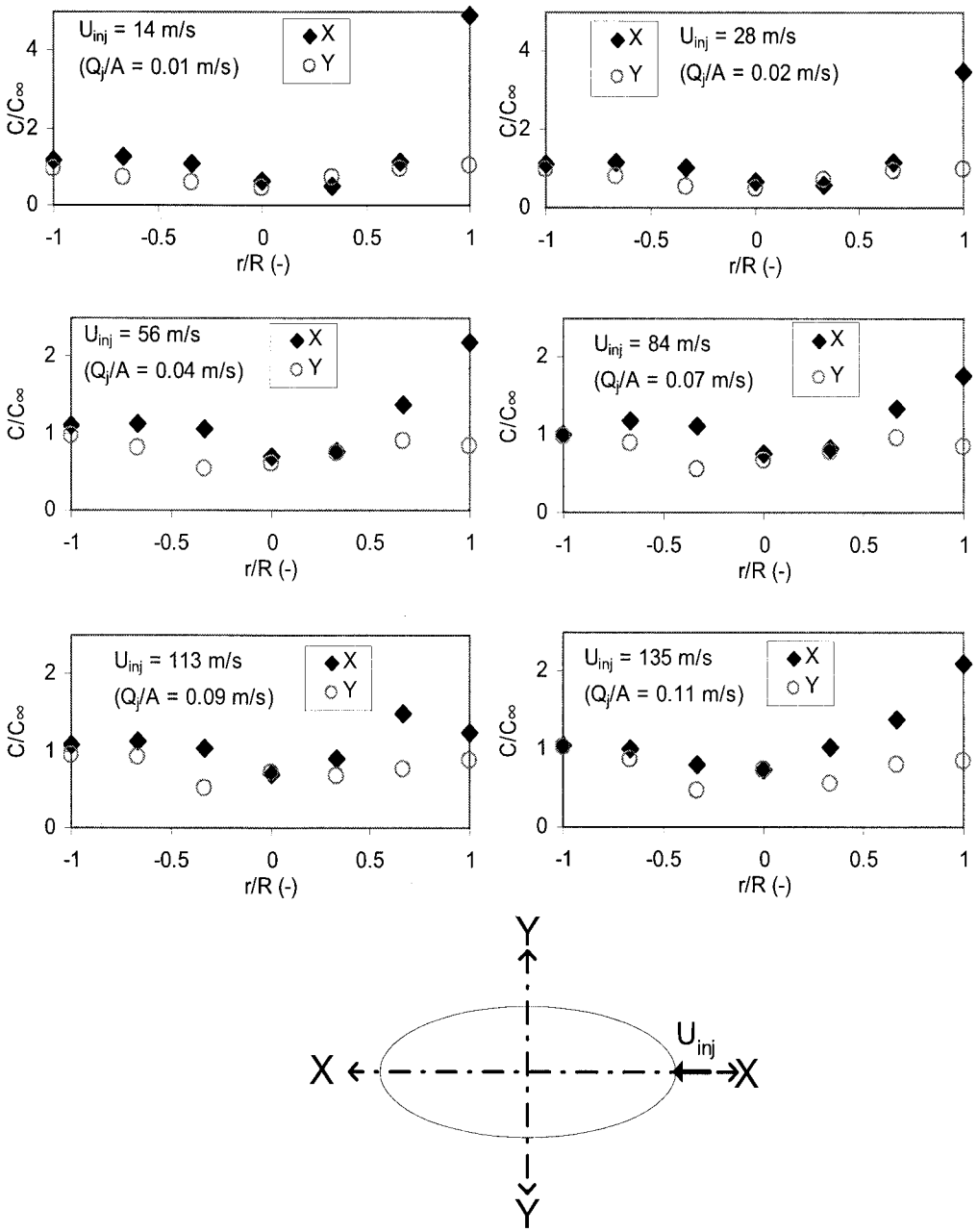

Figure 3. Radial tracer concentration profiles along parallel and perpendicular diameters at the same level as secondary injection for different secondary air injection velocities (U_{inj}).

U_P = 0.1 m/s; H_0 = 1,100 mm; tracer injection at z_j = 560 mm.

charged into the column through a 4.6-mm ID nozzle. Two primary gas superficial velocities were examined (U_P = 0.01 and 0.1 m/s), and the static bed depth was maintained at H_0 = 1010 mm. For each U_P, the secondary air injection velocity was varied from 14 to 135 m/s (Q_j/A = 0.01 to 0.11 m/s), whereas the tracer flow rate was maintained constant.

The tracer concentration was detected by six sampling probes installed at different heights along the bed (below, at, and above the injection level). Each sampling probe consisted of a 15-μm sintered metal filter welded at the end of a 4.6-mm ID stainless steel tube. For each level, two probes were used to measure the helium concentration simultaneously at different radial positions. Each probe could be traversed along the entire column diameter while the system was operating. The helium concentration at the exit of the column, C_∞ (upstream of the cyclone, as shown in Figure 1), was measured by switching the sampling positions between the bed and the column exit using a three-way valve and was used to normalize the concentrations within the bed. A schematic of the setup is shown in Figure 1. Gas samples and reference air were drawn into two TCDs connected to the data-acquisition system.

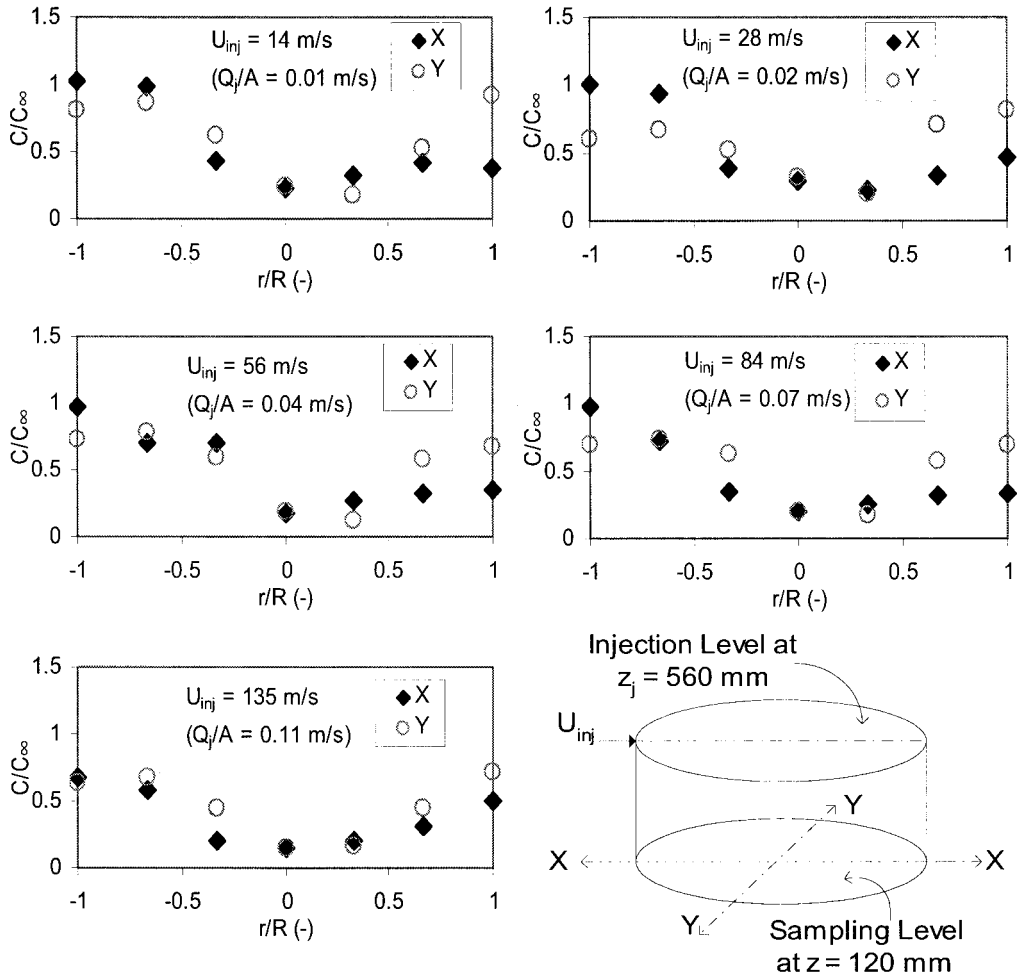

Figure 4. Radial tracer concentration profiles along normal diameters below secondary injection level for different secondary air injection velocities (U_{inj}).

U_P = 0.1 m/s; H_0 = 1,100 mm; tracer injection at z_j = 560 mm; detection at z = 120 mm.

Helium concentration profiles at the secondary air injection level for different secondary air injection velocities from U_{inj} = 14 to 135 m/s (Q_j/A = 0.01 to 0.11 m/s) are shown in Figures 2 and 3 for two primary air superficial gas velocities, U_P = 0.01 and 0.1 m/s, respectively.

Figure 2 shows that the tracer concentration profiles are almost uniform for all secondary feed injection velocities $U_{inj} > 14$ m/s (Q_j/A = 0.01 m/s). However, at U_{inj} = 14 m/s, the radial concentration profile is not uniform, with a higher helium concentration detected near the outer wall. For such a low U_{inj}, the jet penetration distance is very small ($L_j \approx$ 0.01 m), representing the mode where the secondary gas is discharged into the bed as bubbles attached to the near wall. At higher injection velocities the jet penetrated further into the bed creating more uniform radial concentration profiles. The asymmetry in Figure 2(a) in the Y (transverse) direction was probably caused by air maldistribution by the primary distributor at such a low superficial gas velocity.

Compared to the relatively uniform concentration profiles for U_P = 0.01 m/s shown in Figure 2, nonuniform concentration profiles were observed at the higher primary feed flow rate (U_P = 0.1 m/s), as shown in Figure 3. The nonuniform profiles are attributed to a decrease in jet penetration depth at higher U_P (Copan et al., 2001). Both figures show that the profile along a diameter perpendicular to the injection axis was almost uniform for all the cases examined, except for U_{inj} = 14 m/s (Q_j/A = 0.01 m/s). The injected gas clearly spread well beyond the injection axis.

Well below the injection level (z = 120 mm, z_j = 560 mm), the helium was barely detectable for U_P = 0.01 m/s. For U_P = 0.1 m/s, the tracer concentration was higher, as shown in Figure 4, indicating more backmixing at a higher primary flow rate. The effect of secondary gas injection velocity on the backmixing was not very significant.

To examine the uniformity of the injected secondary gas above the injection level, the helium tracer was detected at z = 780 mm, 220 mm above the secondary gas injection level. Concentration profiles were almost uniform, as shown in Figure 5 for U_P = 0.1 m/s. Note that the X–X and Y–Y diameters are at 45° to the injection direction. These results indicate that the secondary gas was well distributed a short distance above the injection level and that U_{inj} had limited influence on the profiles at this height.

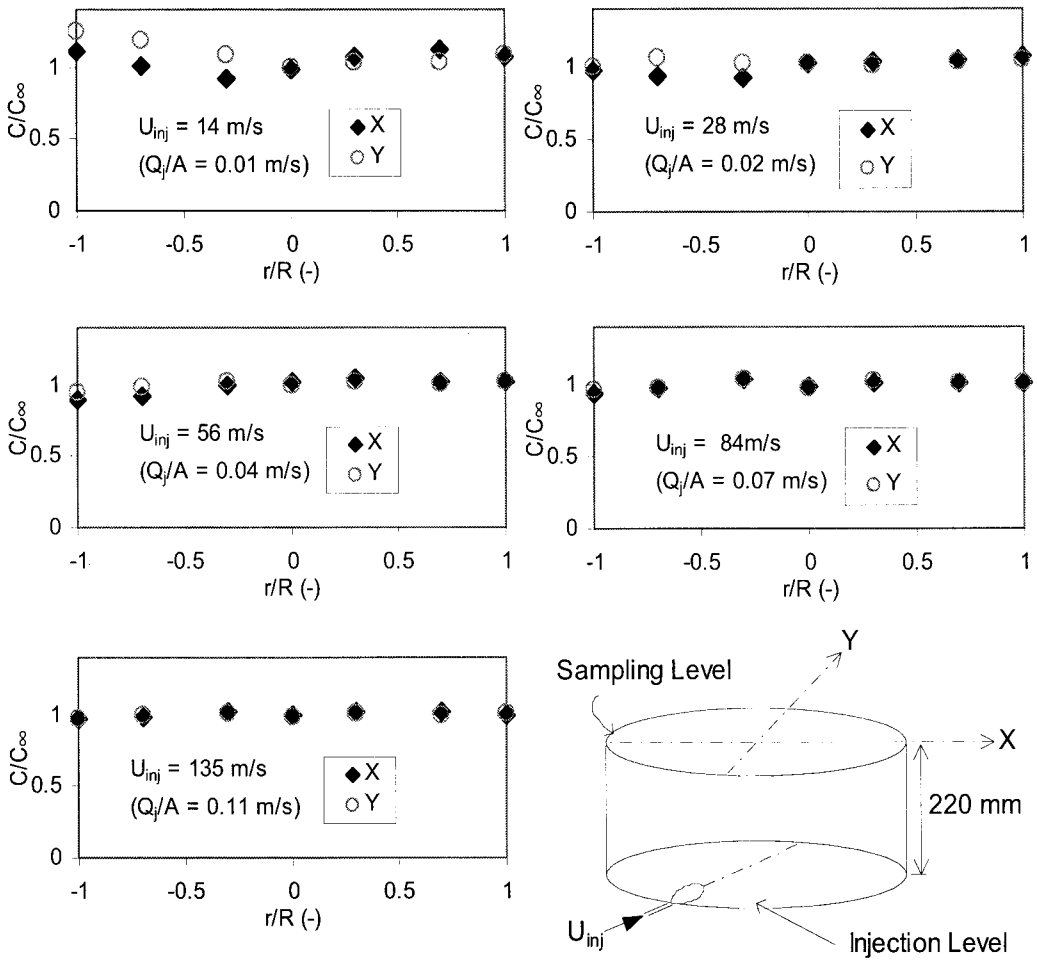

Figure 5. Radial tracer concentration profiles along normal diameters above secondary injection level for different secondary air injection velocities (U_{inj}).

H_0 = 1,100 mm; U_P = 0.1 m/s; tracer injection at z_j = 560 mm; detection at z = 780 mm. In this case, the *X–X* and *Y–Y* diameters are each at 45° to the injection direction.

Unsteady-State Measurements

Residence time distribution (RTD) experiments were conducted using positive step tracer inputs for different primary air superficial gas velocities (0.01 and 0.1 m/s) and secondary air injection velocities (U_{inj} = 0 to 135 m/s; i.e., Q_j/A = 0 to 0.11 m/s). To enable proper mixing of the tracer with either the primary or secondary air before entering the bed, the helium was added upstream of the windbox or injection nozzle, respectively. The measured residence time for tracer added to the primary air included the time in the windbox (V_w = 0.0045 m^3). In addition, the response time for the TCD detection was measured experimentally to be 3.7 s. The TCD was positioned to detect the helium tracer at the bed surface. The tracer injection and detection systems were synchronized using Labtech notebook software so that data logging began at the moment when the solenoid valve controlling the tracer flow was opened. The samples and reference air were drawn continuously into the TCD by the vacuum pump. Using the software, three separate data sets were logged for sampling periods of 200 to 700 s (depending on the operating conditions) at a frequency of 5 Hz.

Each $F(t)$ curve from our experiments is subject to fluctuations and needs to be differentiated to obtain the residence time distribution function, $E(t)$. The measured $F(t)$ data were fitted using the error function (ERF), as follows

$$\mathrm{ERF}(y) = \frac{2}{\sqrt{\pi}} \int_0^y e^{-t^2} dy \tag{1}$$

$$y = \frac{\beta - \varphi t}{t^{0.5}} \tag{2}$$

where β and φ are fitting parameters and t is time. The equation $F(t)$ curve is then

$$F(t) = 0.5[1 - \mathrm{ERF}(y)] \tag{3}$$

The resulting smoothed curves were then differentiated to calculate $E(t)$. Then, the average residence time (τ) and the standard deviation (σ) were calculated from

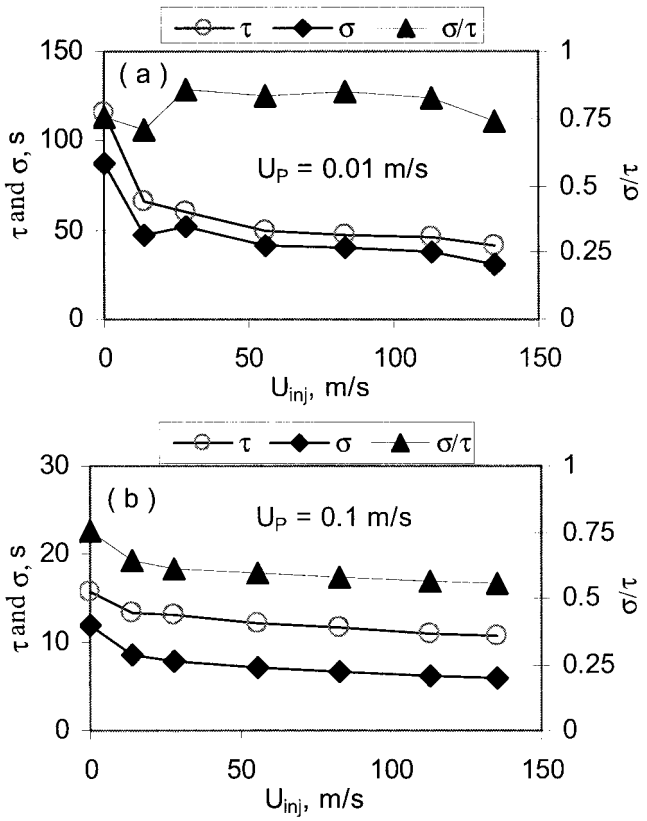

Figure 6. Mean residence time and standard deviation of RTD as functions of U_{inj}.

Secondary air injected at z_j = 560 mm (Q_j/A = 0.0 to 0.11 m/s). Tracer gas injected with primary air. Sampling at: (a) z = 1210 mm for U_P = 0.01 m/s, H = 1160–1230 mm; (b) z = 1420 mm for U_P = 0.1 m/s, H = 1300–1340 mm.

$$\tau = \int_0^\infty tE(t)dt \tag{4}$$

$$\sigma^2 = \int_0^\infty (t-\tau)^2 E(t)dt \tag{5}$$

Helium tracer was injected with the primary feed and detected as close as possible to the bed surface. Experiments were performed for U_P = 0.01 and 0.1 m/s with various secondary injection velocities from 0 to 135 m/s (Q_j/A = 0 to 0.11 m/s). The static bed height was maintained at H_0 = 1100 mm, whereas z_j = 560 mm in all cases.

Sampling at the bed surface required that representative samples be collected covering the entire bed cross section. Ideally several samples should be collected at different radial positions followed by averaging the data to obtain the mean concentration at the bed surface. Three experiments each were performed for U_P = 0.01 and 0.1 m/s without secondary injection and for U_P = 0.01 m/s with U_{inj} = 56 m/s (Q_j/A = 0.04 m/s) at z_j = 560 mm. Helium tracer was injected with the primary air for all three experiments, and five samples were collected at different radial positions at the bed surface in each case. Given the uniformity of the concentrations and the time and tracer required to sample from many points, the concentration at the bed surface was assumed to be uniform and a single sample at the center of the bed surface was subsequently deemed to be sufficient to derive a RTD representative of the entire bed cross section.

Experiments were performed at U_P = 0.01 and 0.1 m/s, with the secondary injection velocity U_{inj} varied from 0 to 135 m/s (Q_j/A = 0 to 0.11 m/s) at z_j = 560 mm. Helium tracer was injected with the primary air for all experiments, with samples collected near the expanded bed surface. The resulting values of τ, σ, and σ/τ are plotted in Figure 6 as functions of U_{inj}. In general, the average residence time τ decreased as U_{inj} increased, both for U_P = 0.01 and 0.1 m/s. However, the decrease is not significant for $U_{inj} > 56$ m/s ($Q_j/A > 0.04$ m/s). A similar trend is observed for the standard deviation σ. The results indicate that so long as the injected gas flow is sufficient to enter as a jet, U_{inj} has little impact on the average gas residence time and standard deviation.

Effect of secondary-to-primary gas-flow ratio (R_{SP}) at constant total superficial gas velocity (U_T)

The RTD was measured without secondary air injection for different primary superficial gas velocities ($U_T = U_P$ = 0.02 to 0.12 m/s) with helium tracer injected into the primary air just

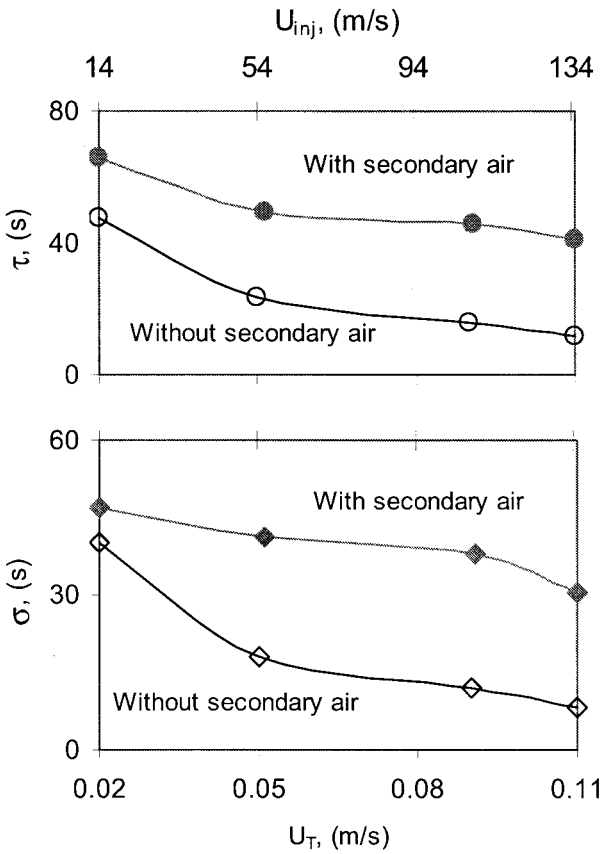

Figure 7. Mean residence time and standard deviation of RTD as functions of U_T.

Open symbols: no secondary injection; closed symbols: with secondary air injection at z_j = 560 mm with U_P fixed at 0.01 m/s; tracer injected with primary air; sampling just above bed surface; H_0 = 1100 mm.

upstream of the windbox. The RTD was then measured for U_T = 0.02 to 0.12 m/s with constant primary air superficial velocity (U_P = 0.01 m/s), whereas secondary air was injected 560 mm above the distributor with U_{inj} = 14, 56, 113, and 135 m/s (Q_j/A = 0.01, 0.04, 0.09, and 0.11 m/s). For the same total feed flow rate, injecting part of the total gas flow 560 mm above the distributor significantly increased the average residence time and standard deviation, as shown in Figure 7. This was expected because the primary flow was reduced when secondary air was injected, and gas elements entering with the primary stream therefore had longer residence times inside the bed.

Modeling

In the present work a dense phase diffusion model (May, 1959; Van Deemter, 1961), based on a two-phase model, is extended to simulate the effect of secondary gas injection into a bubbling fluidized bed. The predictions are then compared with data from the RTD experiments discussed above. Two models are considered. Model I considers only changes in the overall superficial gas velocity at each injection level, whereas Model II considers both changes in total superficial gas velocity and interaction between the jet region caused by the secondary gas and the fluidized material. The dense phase axial diffusion model, referred to here as the *Base Model*, is used to simulate the RTD experiments without secondary gas injection, and provides the limit to both Model I and Model II as the secondary injection approaches zero.

Because the volume of the windbox (V_w = 0.0045 m^3) (see Figure 1) is about 20% of the dense bed volume in our experiments, the windbox is included as a separate continuous stirred-tank reactor (CSTR). In addition, a correction was made for the response of the TCD/sampling system when comparing model and experimental results.

Base model

Model equations for an unsteady-state nonreactive system are derived by writing bubble-phase and dense-phase mole balances for a slice of the bed of height Δz and unit cross-sectional area:

(a) Bubble Phase

$$\Phi_b(1-\alpha_b)\frac{\partial C_b}{\partial t}+\frac{Q_b}{A}\frac{\partial C_b}{\partial z}-\Phi_b D_{ab}\frac{\partial^2 C_b}{\partial z^2}+k_{bd}a_b(C_b-C_d)=0 \quad (6)$$

(b) Dense Phase

$$\Phi_d(1-\alpha_d)\frac{\partial C_d}{\partial t}+\frac{Q_d}{A}\frac{\partial C_d}{\partial z}-\Phi_d D_{ad}\frac{\partial^2 C_d}{\partial z^2}+k_{bd}a_b(C_d-C_b)=0 \quad (7)$$

To simplify the model, the following assumptions are adopted:

(1) Bubbles are free of solids so that $\alpha_b = 0$ and $\Phi_b = \varepsilon_b$.

(2) Gas is distributed between the phases according to the two-phase model.

(3) Bubble phase gas is in plug flow (i.e., $D_{ab} = 0$), whereas it is axially dispersed in the dense phase with D_{ad}, given (Lee and Kim, 1989) by

$$\mathrm{Pe}_a=\frac{U_T D}{D_{ad}}=0.02566\left(\frac{U_T}{U_{mf}}\right)^{-0.54}\left(\frac{\rho_p}{\rho_g}\right)^{0.067}\left(\frac{d_p}{D}\right)^{-0.588} \quad (8)$$

Because this correlation was developed to account for overall dispersion, D_{ad} was divided by $(1-\varepsilon_b)$ to estimate the dispersion coefficient for the dense phase alone.

(4) The volumetric interphase mass transfer coefficient is calculated using the equation of Sit and Grace (1981)

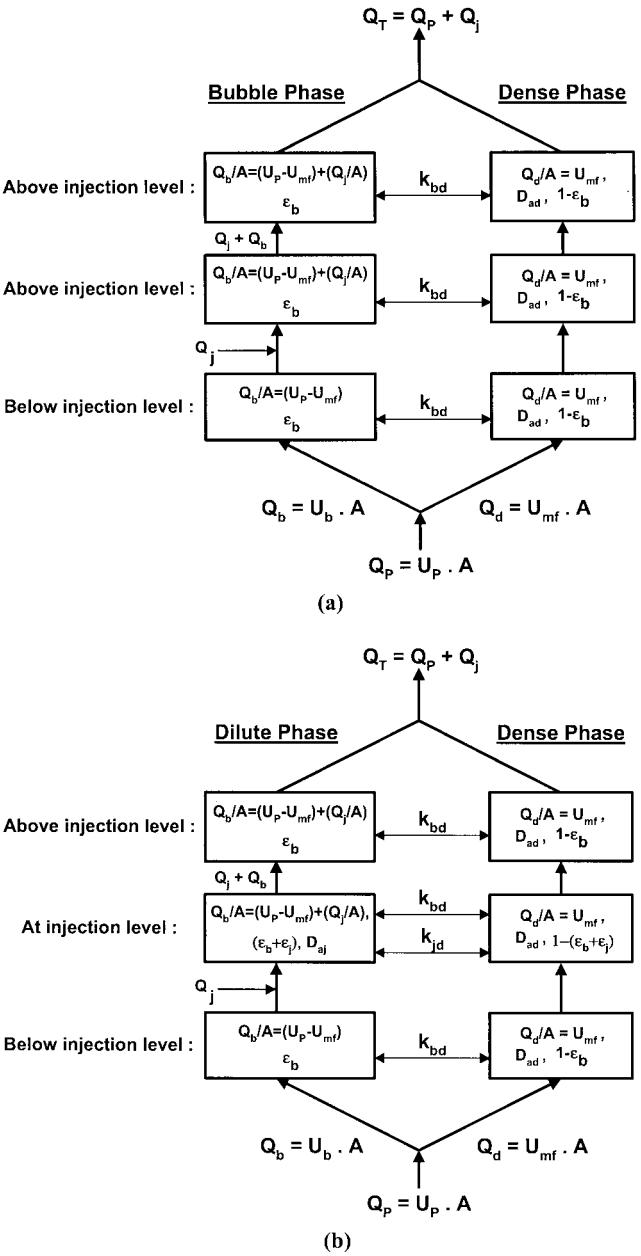

Figure 8. Phase flows, dispersion, and hold-ups for (a) Model I and (b) Model II.

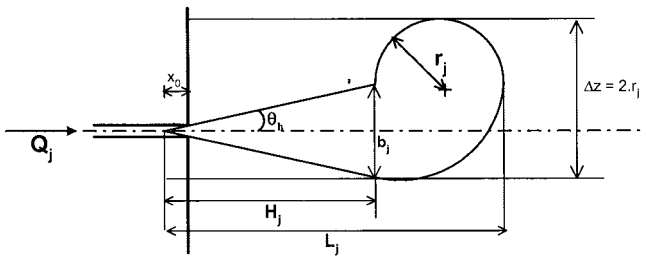

Figure 9. Assumed jet region geometry.

$$k_{bd}a_b = \frac{6\varepsilon_b}{d_b}\left[\frac{U_{mf}}{3} + 2\left(\frac{D_e\varepsilon_{mf}U_b}{\pi d_b}\right)^{1/2}\right] \tag{9}$$

Bubble size and velocity (d_b and u_b) are allowed to increase with height. However, the bubble size is not allowed to exceed the maximum stable bubble size $d_{b\,\max}$, given by

$$d_{b\,\max} = 2\frac{(u_t^*)^2}{g} \tag{10}$$

where u_t^* is the terminal settling velocity of a single particle of diameter $2.7d_p$ in the fluidizing gas.

(5) Adsorption is neglected.

(6) The dense phase bed voidage $= \varepsilon_{mf}$ throughout the bed.

With the above assumptions, Eqs. 6 and 7 become

Bubble Phase

$$\varepsilon_b\frac{\partial C_b}{\partial t} + \frac{Q_b}{A}\frac{\partial C_b}{\partial z} + k_{bd}a_b(C_b - C_d) = 0 \tag{11}$$

Dense Phase

$$\varepsilon_d(1-\varepsilon_b)\frac{\partial C_d}{\partial t} + \frac{Q_d}{A}\frac{\partial C_d}{\partial z} - (1-\varepsilon_b)D_{ad}\frac{\partial^2 C_d}{\partial z^2} + k_{bd}a_b(C_d - C_b) = 0 \tag{12}$$

Initial Conditions

@ $t = 0$,

$$C_b = C_d = 0 \tag{13}$$

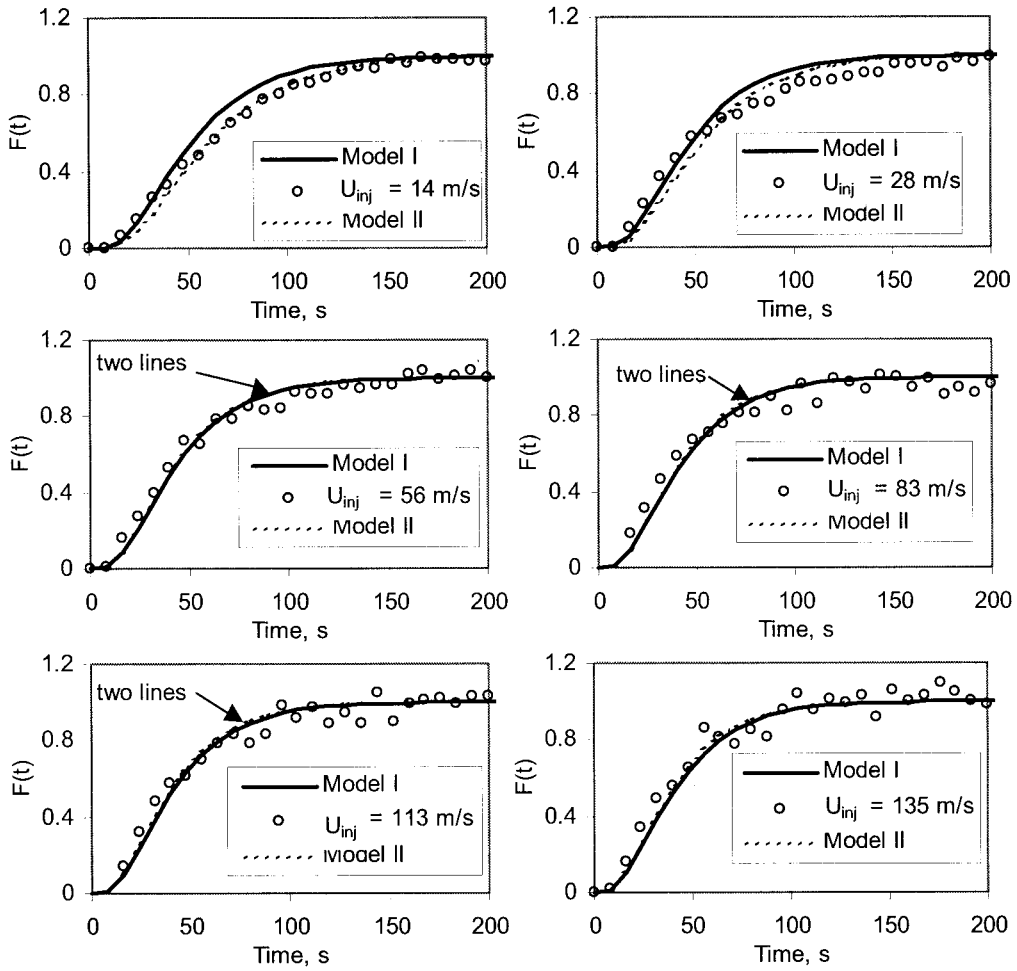

Figure 10. Comparison between $F(t)$ predicted by Models I and II for U_P = 0.01 m/s and U_{inj} = 14 to 135 m/s.

Secondary air injected through one nozzle at z_j = 560 mm (Q_j/A = 0.01 to 0.11 m/s); tracer injected with primary air and detected at z = 1,210 mm; H_0 = 1,100 mm.

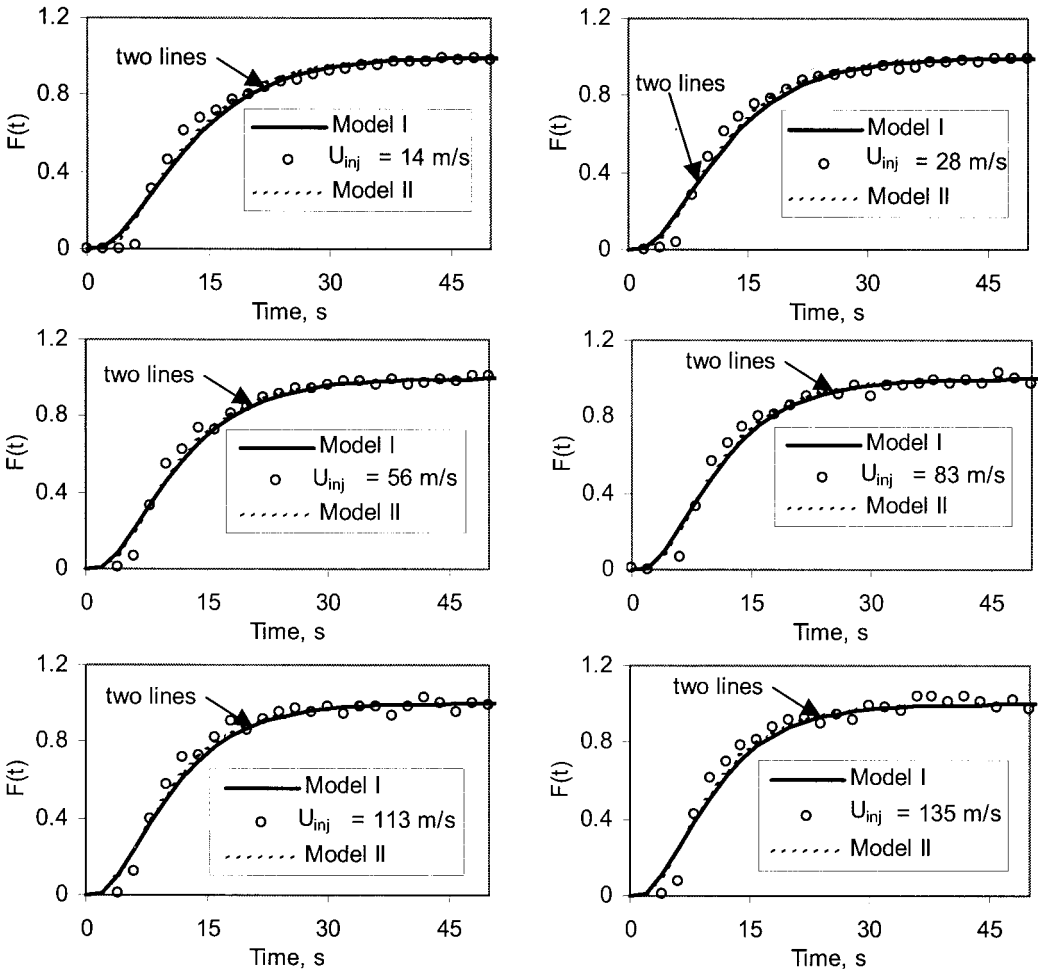

Figure 11. Comparison between *F*(*t*) predicted by Models I and II for U_P = 0.1 m/s and U_{inj} = 14 to 135 m/s.

Secondary air injected through one nozzle at z_j = 560 mm (Q_j/A = 0.01 to 0.11 m/s); tracer injected with primary air and detected at z = 1,420 mm; H_0 = 1,100 mm.

Boundary Conditions

For $t > 0$

@ $z = 0$,

$$C_b = C_0 \tag{14}$$

$$C_d = \frac{D_{ad}(1-\varepsilon_b)A}{Q_d}\frac{\partial C_d}{\partial z} + C_0 \tag{15}$$

C_0 is the windbox outlet concentration given for a positive step change by

$$C_0 = C_i e^{-t/\tau_w} \tag{16}$$

where C_i is the windbox inlet concentration, and τ_w is the windbox mean residence time. @ $z = H$,

$$\frac{\partial C_d}{\partial z} = 0 \tag{17}$$

The outlet concentration is calculated from

$$C_H = \frac{Q_b C_b + Q_d C_d}{Q_P} \tag{18}$$

The mean bubble diameter as a function of height and operating conditions is estimated by the Mori and Wen (1975) correlation, whereas the bubble diameter at the distributor plate is calculated from the Miwa et al. (1972) correlation.

Equations 11 and 12 were solved numerically using Visual FORTRAN 5.0. The partial differential equations were solved using the subroutine MOLCH, which uses the method of lines (Constantinides and Mostoufi, 1999).

Models for simulating secondary gas injection

The base model (without secondary gas) is modified when secondary gas is injected horizontally into a bubbling bed above the distributor plate. In the base model, radial dispersion was assumed to be negligible so that radial concentration profiles at any height above the distributor are assumed to be uniform. However, when secondary feed is injected, this assumption might not be valid, especially for a low injection velocity [<14 m/s (Q_j/A = 0.01 m/s)] where the

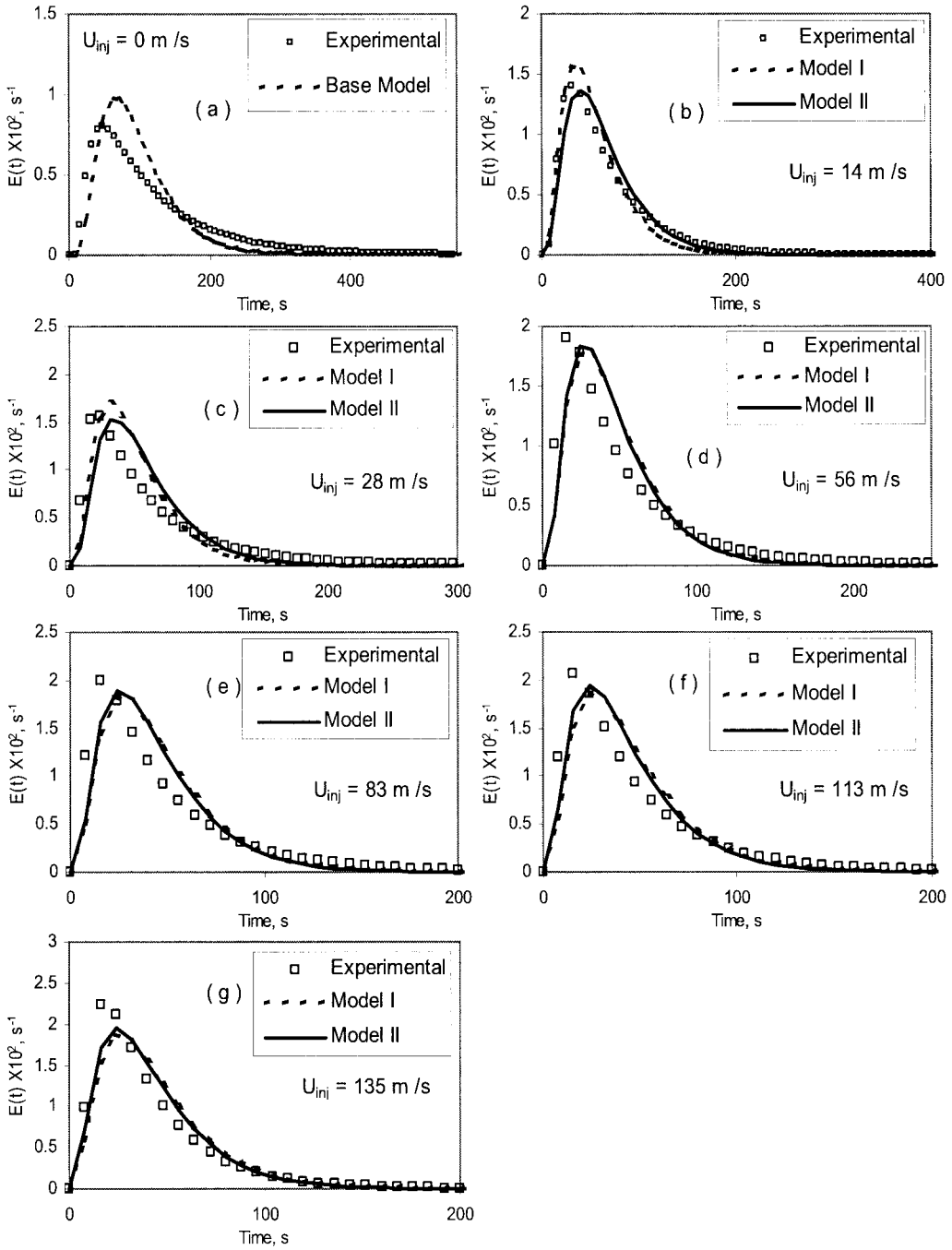

Figure 12. Comparison between experimental residence time distributions and models (Base Model, Models I and Model II) prediction for U_P = 0.01 m/s: (a) without any secondary injection; (b) to (g) for U_{inj} = 14 to 135 m/s.

Secondary air injected through one nozzle at z_j = 560 mm (Q_j/A = 0.01 to 0.11 m/s); tracer injected with primary air and detected at z = 1,210 mm; H_0 = 1,100 mm.

concentration was nonuniform near the injection nozzle. However, the experiments reported earlier show that a uniform distribution was achieved within a short distance above the injection level for the relatively small column used, where the jet penetration was of the same order as the column diameter. Therefore, using the base model to simulate the regions above and below the injection level, with provision to change the total flow above the injection level, is a reasonable first approximation. Note, however, that this approach is unlikely to be sufficient in cases where the jet penetration is much less than the column cross-sectional dimension.

In Model I, all secondary gas is assumed to be distributed immediately in a uniform manner across the entire injection level, with all of the secondary gas added to the bubble phase. The base model equations are then solved up to the

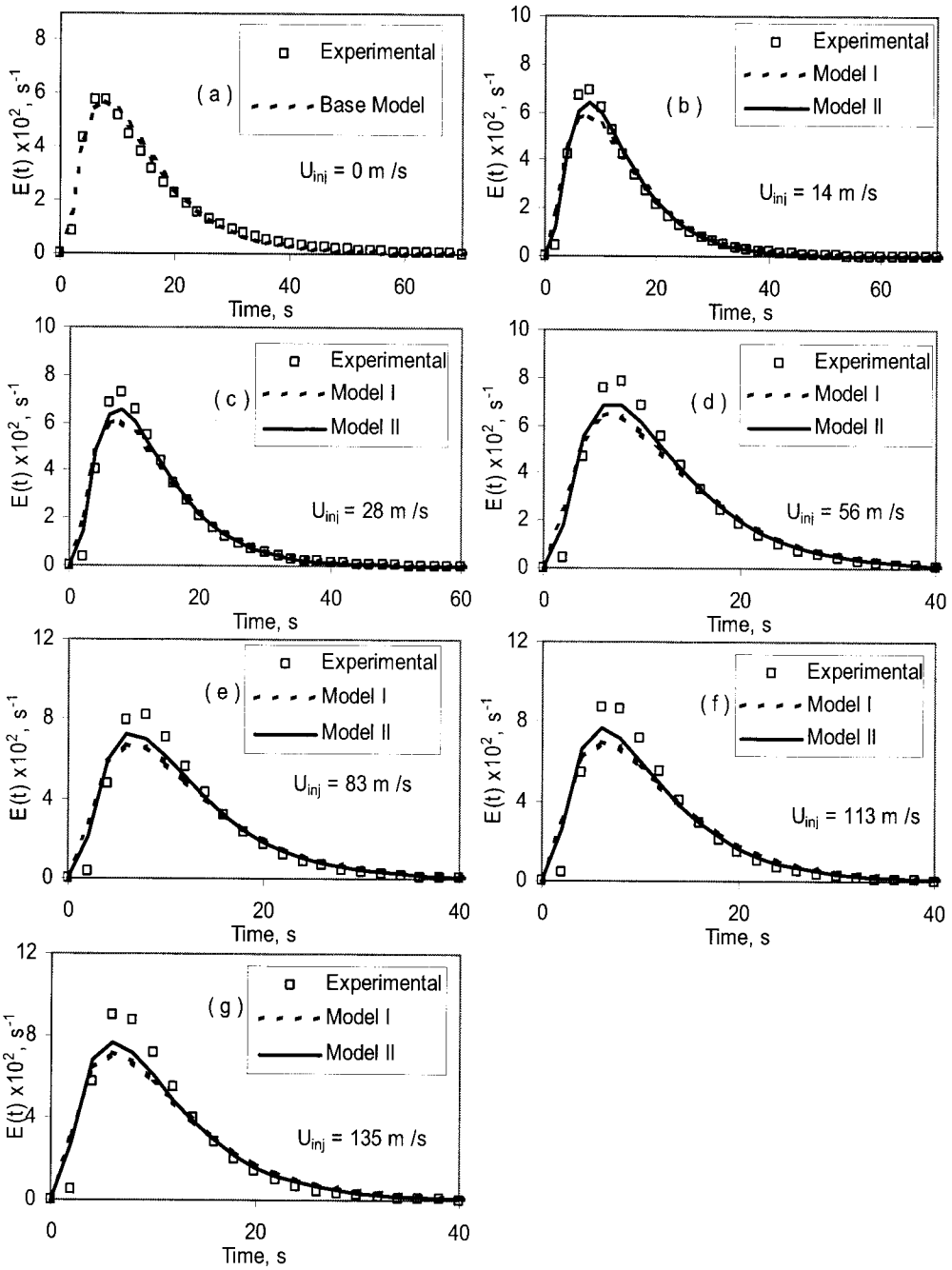

Figure 13. Comparison between experimental residence time distributions and models (Base Model, Models I and Model II) predictions for U_P = 0.1 m/s: (a) without any secondary injection; (b) to (g) for U_{inj} = 14 to 135 m/s.

Secondary air injected through one nozzle at z_j = 560 mm (Q_j/A = 0.01 to 0.11 m/s); tracer injected with primary air and detected at z = 1420 mm; H_0 = 1100 mm.

injection level. At the secondary injection level, the parameters in Eqs. 11 and 12 are recalculated after adjusting the volumetric flow of the bubble phase to include the secondary gas ($Q_b + Q_j$). In addition, the bubble diameter is adjusted using the Mori and Wen correlation, assuming that the initial bubble size d_{b0} equals d_b calculated just below the injection level. From this height up to the bed surface, one then proceeds with revised values of Q_T, Q_b, d_b, and $z' = z - z_j$. D_{ad} is assumed to be the same above and below z_j. Axial dispersion and total exchange rate are calculated as for the base model. Figure 8a shows the secondary feed injection for Model I.

The assumptions of Model I are applied again in Model II above and below the jet injection level(s). However, in this model, to provide a better representation of the zone where secondary injection occurs, three phases are assumed at the injection level: bubbles, dense phase, and jet, as shown in

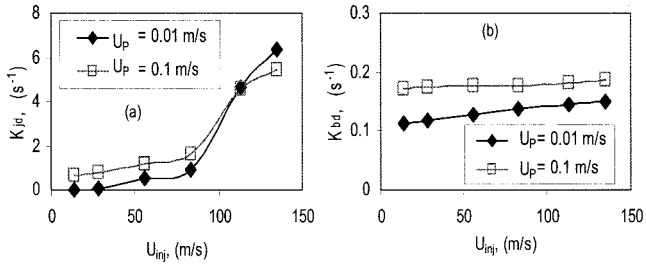

Figure 14. Volumetric mass-transfer coefficients as functions of U_{inj}: (a) fitted K_{jd}; (b) averaged K_{bd} for the entire bed. Secondary air injected at z_j = 560 mm (Q_j/A = 0.01 to 0.11 m/s); tracer injected with primary air and detected at: (a) z = 1210 mm and (b) z = 1420 mm; H_0 = 1100 mm.

Figure 8b. At this level, the bubble and jet phases are lumped together at the injection level

$$(\varepsilon_b + \varepsilon_j)\frac{\partial C_{bj}}{\partial t} + \frac{(Q_b + Q_j)}{A}\frac{\partial C_{bj}}{\partial z} + (k_{bd}a_b + k_{jd}a_j)(C_{bj} - C_d) = 0 \quad (19)$$

Here ε_j is the fraction of the injection level volume occupied by the jet, k_{jd} is the mass-transfer coefficient between the jet and dense phase, and a_j is the surface area of interphase boundary of the jet per unit injection level volume; k_{jd} is considered as the fitting parameter, whereas a_j and ε_j are based on geometry. The jet region volume V_j is estimated based on the assumption that the jet is composed of a cone and a sphere attached to the base of the cone (Xuereb and Laguérie, 1991), as shown in Figure 9. The apex of the cone is a distance x_0 upstream of the end of the injection nozzle. The total jet volume is

$$V_j = V_{cone} + V_{sphere} \quad (20)$$

with

$$V_{cone} = \frac{\pi}{3} H_j b_j^2 \quad (21)$$

and

$$b_j = H_j \tan(\theta_h) \quad (22)$$

$$V_{sphere} = \frac{4}{3}\pi r_j^3 \quad (23)$$

H_j, the cone height, is taken as (L_j/1.6), as suggested by Shakhova and Minayev (1972). L_j, the jet penetration depth, is calculated by the correlation of Merry (1971). The jet half-angle θ_h is assumed to be constant and equal to 6.25° (Merry, 1971). The radius of the sphere (r_j) formed at the end of the jet region is taken as (H_j/1.8), as suggested by Shakhova and Minayev (1972). The volume of the injection level is taken as $V_{inj} = \pi D^2 r_j/2$. The interphase area per unit volume of the jet boundary a_j is set equal to the (surface area of the cone + surface area of the sphere)/V_{inj}. The fraction of volume occupied by the jet in this zone is simply

$$\varepsilon_j + V_j/V_{inj} \quad (24)$$

For the dense phase, Eq. 14 is modified to account for the jet as follows:

$$\varepsilon_{mf}[1 - (\varepsilon_j + \varepsilon_b)]\frac{\partial C_d}{\partial t} + \frac{Q_d}{A}\frac{\partial C_d}{\partial z} - [1-(\varepsilon_j+\varepsilon_b)]D_{aj}\frac{\partial^2 C_d}{\partial z^2} + (k_{bd}a_b + k_{jd}a_j)(C_d - C_{bj}) = 0 \quad (25)$$

The axial dispersion coefficient D_{aj}, in the jet region, is considered a fitting parameter.

Model predictions

The base model (that is, model without secondary injection) is used to predict $F(t)$ for the experiments performed without secondary gas for U_P = 0.01 to 0.12 m/s. As shown elsewhere (Al-Sherehy, 2002), the base model gave reasonable fits to the experimental data within the range examined. No fitting parameters beyond those incorporated in existing correlations are required for this model because all model parameters are calculated from the correlations presented above. Hence, the base model provides a good foundation for extension to cases with secondary gas injection.

Model I is solved without any fitting parameters, whereas Model II involves two fitting parameters (k_{jd} and D_{adj}) at the injection level, although there are no fitting parameters for the regions above and below the injection level. Figures 10 and 11 compare the model predictions and experimental $F(t)$ for U_P = 0.01 and 0.1 m/s at various values of U_{inj} from 14 to 135 m/s (Q_j/A = 0.01 to 0.11 m/s). Figures 12 and 13 compare the residence time distribution, $E(t)$. Both models are seen to fit the experimental data quite well, with differences between the predictions of the two models being relatively small.

Although Model I is simpler, Model II provides a better representation of the jet region, aided by having two parame-

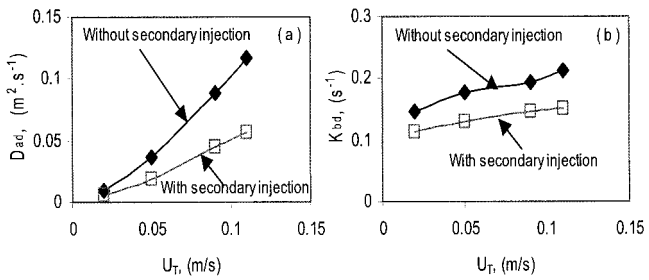

Figure 15. K_{bd} and D_{ad} as functions of total superficial gas velocity for the bubbling bed without and with secondary gas injection.

Tracer gas was injected with the primary air; secondary air injected at z_j = 560 mm; H_0 = 1,100 mm. Values with secondary injection are averaged from data with U_{inj} = 14, 56, 113, and 135 m/s (Q_j/A = 0.01, 0.04, 0.09, and 0.11 m/s).

ters to fit. Model II provides a good basis for adding more complexity to the model, as needed.

The fitted interphase mass-transfer coefficient between the jet and the dense phase is plotted in Figure 14(a) as a function of the secondary gas injection velocity for $U_P = 0.01$ and 0.1 m/s. In both cases K_{jd} ($=k_{jd}a_j$) increased with increasing U_{inj}. This is expected because increasing the injection velocity increases the jet penetration depth and hence increases the interfacial area between the dense and jet phases. A significant increase in K_{jd} is observed for $U_{inj} = 113$ and 135 m/s ($Q_j/A = 0.09$ and 0.11 m/s). At such injection velocities the jet penetration depth is comparable to the bed diameter. Note that k_{jd} used to fit Model II is in the range of 0.01 to 0.8 m/s, comparable to the range reported in the literature for jet-to-dense phase mass transfer in the grid zone (0.1 to 1.0 m/s) (Grace, 1986).

Figure 14b shows that the average volumetric bubble-to-dense phase mass transfer coefficient for the entire bed is not influenced significantly by secondary feed, especially at higher U_P. In addition, the interphase mass transfer coefficient for the injection level is an order of magnitude higher than that for the other zones inside the bed. The axial dispersion coefficient D_{aj} used to fit the model was found to be very small (1×10^{-6} m^2/s), suggesting that axial mixing in the jet region is too small for it to be needed in the model.

Comparison of bubbling bed with and without secondary air

Gas mixing for the bubbling bed with and without secondary feed injection and the same total feed flow rate are explored here using the volumetric mass transfer coefficients K_{bd} and axial dispersion coefficients D_{ad}. The RTD was measured without secondary feed injection for different primary superficial gas velocities ($U_T = U_P = 0.02$ to 0.12 m/s) with tracer injected with the primary air. The RTD was then measured for $U_T = 0.02$ to 0.12 m/s with constant primary air flow ($U_P = 0.01$ m/s) and with secondary air injected 560 mm above the distributor with $U_{inj} = 14$, 56, 113, and 135 m/s, whereas tracer was injected with the primary feed.

K_{bd} and axial dispersion coefficients D_{ad} are predicted by the models using the literature correlations above (Eqs. 8 and 9). Because both are predicted to change with height, an arithmetic average value for the entire bed (below and above the injection point) was calculated and plotted as a function of U_T in Figure 15 for cases with and without secondary air injection. D_{ad} and K_{bd} are both seen to be significantly smaller with secondary air injection than without. This decrease is attributed to both bubble diameter and hold-up decreasing with decreasing U_P as secondary gas is injected. This suggests that with secondary gas the bed contains smaller bubbles, which is consistent with the smaller pressure fluctuations and standard deviations (Al-Sherehy, 2002) when part of the total gas flow was injected as secondary feed.

Conclusions

When secondary gas was injected horizontally into a bubbling fluidized, the gas distribution was nonuniform at the injection level, especially at smaller injection velocities. However, injected tracer became uniformly distributed within a short distance above the injection level. Gas backmixing did not increase significantly when secondary feed was injected for the conditions explored in this work.

The mean residence time and standard deviation were not affected significantly by the secondary feed injection velocity at higher U_{inj}. However, significant changes were observed when part of the total gas flow was injected as a secondary stream. This led to significant increase in average residence time and standard deviation for the range of conditions studied.

Two two-phase models are proposed to simulate secondary gas injection. Model I features a step change in total flow at the injection level, whereas Model II is more complex, with allowance for the jet geometry and for different interphase mass transfer near the injection level. Both models are shown to give reasonable agreement with the experimental gas mixing results obtained in a column of 152 mm diameter.

Notation

A = column cross-sectional area, m^2
a_b = specific surface area of gas bubble, m^2/m^3
a_j = specific surface area of jet boundary, m^2/m^3
b_j = cone base shown in Figure 9 and given by Eq. 22, m
C = concentration, mol/m^3
C_∞ = concentration at column exit, mol/m^3
D = column diameter, m
D_a = axial dispersion coefficient, m^2/s
D_{ab} = axial dispersion coefficient in bubble phase, m^2/s
D_{ad} = axial dispersion coefficient in dense phase, m^2/s
D_{adj} = axial dispersion coefficient in jet region, m^2/s
D_{ij} = binary diffusion coefficient of component i diffusing into component j, m^2/s
D_m = effective diffusivity of gas mixture, m^2/s
D_r = radial dispersion coefficient, m^2/s
d_b = bubble diameter, m
d_{bmax} = maximum stable bubble diameter, m
d_o = jet injection nozzle diameter, m
d_p = mean particle diameter, m
ERF = error function given by Eq. 1
$E(t)$ = residence-time distribution function, s^{-1}
$F(t)$ = fraction of gas leaving column during residence time of 0 to t
g = gravitational acceleration, m/s^2
H = bed height, m
H_0 = static bed height, m
H_j = length of cone shown in Figure 9, m
K_{bd} = volumetric mass transfer coefficient between bubble and dense phase, s^{-1}
K_{jd} = volumetric mass transfer coefficient between jet and dense phase, s^{-1}
k_{bd} = interphase mass exchange coefficient between bubble and dense phase, m s^{-1}
k_{jd} = interphase mass exchange coefficient between jet and dense phase, m s^{-1}
L_j = jet penetration length (see Figure 9), m
N_{or} = number of orifices in the grid
Pe_a = Peclet number for dispersion in axial direction, UR/D_a
Q = volumetric flow rate, m^3/s
R = column radius, m
R_{SP} = secondary-to-primary feed flow ratio
r = radial coordinate, m
r_j = radius of sphere formed at end of jet, Figure 9, m
t = time, s
U_b = bubble velocity, m/s
U_{inj} = secondary feed injection velocity, m/s
U_{mb} = superficial gas velocity at minimum bubbling, m/s
U_{mf} = superficial gas velocity at minimum fluidization, m/s
U_P = primary feed superficial gas velocity, m/s
U_T = total superficial gas velocity, m/s
u_t^* = terminal settling velocity of a single particle given in Eq. 10, m/s
V_{inj} = volume of jet level, m^3
V_j = volume of jet given by Eq. 20, m^3
X, Y = radial coordinates as shown in Figure 3, m
y = error function parameter given by Eq. 2
z = vertical coordinate, m
z_j = height of injection nozzle above distributor, m

Greek letters

α_b, α_d = fraction of bubble and dense phase volumes occupied by solids
β = fitting parameter for Eq. 2
ρ_p = particle density, kg/m^3
ε_{mf} = bed voidage at minimum fluidization
ε_{mb} = bed voidage at minimum bubbling
ε_j = volume fraction of injection level slice occupied by jets
φ = fitting parameter, Eq. 2
θ_h = jet half-angle, Figure 9, degrees
ρ_g = gas density, kg/m^3
ε_d = dense phase voidage
ε_b = volume fraction of bed occupied by bubbles
Φ_b, Φ_d = fraction of bed volume occupied by bubble and dense phase
σ = standard deviation of gas RTD, s
μ = gas viscosity, kg m^{-1} s^{-1}
τ = average gas residence time, s

Subscripts

b = bubble phase
d = dense phase
0 = primary feed
H = at height H
i = component i
j = jet
P = primary feed
T = total feed
w = windbox

Abbreviations

CSTR = continuous stirred-tank reactor
FCC = fluid catalytic cracking
PSD = particle size distribution
RTD = residence time distribution

Literature Cited

Al-Sherehy, F., "Distributed Addition of Gaseous Reactants in Fluidized Beds," PhD Thesis, University of British Columbia, Vancouver (2002).

Bramer, E. A., "Flue Gas Emission from Fluidized Bed Combustion, Atmospheric Fluidized Bed Coal Combustion Research, Development and Application," *Coal Sci. Technol.*, **22**, 51 (1995).

Choudhary, V. R., S. T. Chaudhari, A. M. Rajput, and V. H. Rane, "Beneficial Effect of Oxygen Distribution on Methane Conversion and C2-Selectivity in Oxidative Coupling of Methane to C2-Hydrocarbons over Lanthanum-Promoted Magnesium Oxide," *J. Chem. Soc. Chem. Commun*., 1526 (1989).

Constantinides, A., and N. Mostoufi, *Numerical Methods for Chemical Engineers with MATLAB Applications*, Prentice Hall, Upper Saddle River, NJ (1999).

Contractor, R. M., and A. W. Sleight, "Selective Oxidation in Riser Reactor," *Catal. Today* **3**, 175 (1988).

Copan, J., N. Clarke, and F. Berruti, "The Interaction of Single and Two-Phase Jets and Fluidized Beds," in *Fluidization X*, M. Kwauk, J. Li, and W.-C. Yang, eds., Engineering Foundation, New York, pp. 77–84 (2001).

Coronas, J., M. Menendez, and J. Santamaria, "Use of a Ceramic Membrane Reactor for the Oxidative Dehydrogenation of Ethane to Ethylene and Higher Hydrocarbons," *Ind. Eng. Res.*, **34**, 4229 (1995).

Grace, J. R., "Fluid Bed as a Chemical Reactor," Chapter 13 in *Gas Fluidization Technology*, D. Geldart, ed., Wiley, Chichester, UK (1986).

Grace, J. R., "Influence of Riser Geometry on Particle and Fluid Dynamics in Circulating Fluidized Bed Risers," in *Circulating Fluidized Bed Technology V*, M. Kwauk and J. Li, eds., Science Press, Beijing (1997).

Lee, G. S., and S. D. Kim, "Gas Mixing in Slugging and Turbulent Fluidized Beds," *Chem. Eng. Commun.*, **86**, 91 (1989).

Lummi, A. P., and A. P. Baskakov, *Khim. Prom*., No. 522, *J. Eng. Phys*., 32 (1967).

May W.G., "Fluidized-Bed Reactor Studies," *Chem. Eng. Prog.*, **55**(12), 49 (1959).

Merry, J. M. D., "Penetration of a Horizontal Gas Jet into a Fluidized Bed," *Trans. Inst. Chem. Eng*., **49**, 189 (1971).

Miwa, K., S. Mori, T. Kato, and I. Muchi, "Behaviour of Bubbles in Gaseous Fluidized Bed," *Int. Chem. Eng*., **12**, 187 (1972).

Mori, S., and C. Y. Wen, "Estimation of Bubble Diameter in Gaseous Fluidized Beds," *AIChE J.*, **21**, 109 (1975).

Potter, O. E., "Mixing," Chapter 7 in *Fluidization*, J. F. Davidson and D. Harrison, eds., Academic Press, London, pp. 293–381 (1971).

Reid, R. C., J. M. Prausnitz, and T. K. Sherwood, *The Properties of Gases and Liquids*, McGraw Hill, New York (1977).

Shakhova, N. A., and G. A. Minayev, "Aerodynamics of Jets Discharged into Fluidized Beds," *Heat Transfer-Sov. Res*., **4**(1), 133 (1972).

Sit, S. P., and J. R. Grace, "Effect of Bubble Interaction on Interphase Mass Transfer in Gas Fluidized Beds," *Chem. Eng. Sci*., **36**, 327 (1981).

Tonkovich, A. L. Y., J. L. Zilka, D. M. Jimenez, G. L. Roberts, and J. L. Cox, "Experimental Investigations of Inorganic Membrane Reactors: A Distributed Feed Approach for Partial Oxidation Reaction," *Chem. Eng. Sci*., **51**, 789 (1996).

Van Deemter, J. J., "Mixing and Contacting in Gas-Solid Fluidized Beds," *Chem. Eng. Sci*. **13**, 143 (1961).

Xuereb, C., C. Laguérie, and T. Baron, "Etude du Comportement de Jets Continus Horizontaux ou Inclinés Introduits dans un Lit Fluidisé par un Gaz, I: Morphologie des Jets," *Powder Technol*., **67**, 43 (1991a).

Xuereb, C., C. Laguérie, and T. Baron, "Etude du Comportement de Jets Continus Horizontaux ou Inclinés Introduits dans un Lit Fluidisé par un Gaz, II: Profils de Vitesse du Gaz dans les Jets Horizontaux," *Powder Technol*., **64**, 271 (1991b).

Yates, J. G., S. S. Cobbinah, D. J. Cheesman, and S. P. Jordan, "Particle Attrition in Fluidized Beds Containing Opposing Jets," *AIChE Symp. Ser.*, **87**(281), 13 (1987).

Manuscript received Apr. 17, 2003, and revision received Aug. 29, 2003.